C. R. Geoscience 351 (2019) 147–153

Contents lists available at ScienceDirect

Comptes Rendus Geoscience

www.sciencedirect.com

Internal Geophysics (Physics of Earth's interior)

Electrical resistivity of *fcc* phase iron hydrides at high pressures and temperatures

Kenji Ohta [a,*], Sho Suehiro [a], Kei Hirose [b,c], Yasuo Ohishi [d]

[a] Department of Earth and Planetary Sciences, Tokyo Institute of Technology, Meguro, Tokyo, Japan
[b] Earth-Life Science Institute, Tokyo Institute of Technology, Meguro, Tokyo, Japan
[c] Department of Earth and Planetary Science, The University of Tokyo, Bunkyo, Tokyo, Japan
[d] Japan Synchrotron Radiation Research Institute, Sayo, Hyogo, Japan

ARTICLE INFO

Article history:
Received 20 March 2018
Accepted after revision 24 May 2018
Available online 12 November 2018

Handled by James Badro

Keywords:
Iron hydride
Electrical resistivity
Earth's core
Core density deficit

ABSTRACT

We measured the electrical resistivity of face-centered-cubic (*fcc*) structured iron hydrides at high pressures up to 65 GPa and high temperatures in a laser-heated diamond anvil cell. The results indicate that the resistivity of stoichiometric *fcc* FeH_x ($x \sim 1.0$) is smaller than that of *fcc* Fe at the same pressure and temperature conditions. The same behavior was also observed in *fcc* $FeNiH_x$ ($x \sim 1.0$). On the other hand, hydrogen-poor *fcc* FeH_x ($x < 0.77$) showed a resistivity comparable to that of the *fcc* phase of pure iron. Therefore, we conclude that the stoichiometric *fcc* Fe (–Ni) hydride is more conductive than Fe (–Ni) with the same crystal symmetry, and the impurity resistivity of hydrogen in Fe is vanishingly small. Even if hydrogen is the major light element in the Earth's core, it would have little influence on the electrical and thermal conductivity of Fe–Ni alloys, and hence the thermal evolution of the core.

1. Introduction

The Earth's core is not only composed of iron–nickel (Fe–Ni) alloy, but also needs other lighter impurities to explain the 8–10% density deficit with respect to pure Fe (e.g., Poirier, 1994). Hydrogen as a light element in the Earth's core has been a focus of interest for more than six decades (Badding et al., 1991; Birch, 1952; Fukai and Akimoto, 1983; Iizuka-Oku et al., 2017; Mao et al., 2004; Shibazaki et al., 2012; Stevenson, 1977). Therefore, the effects of hydrogen on crystal structures of Fe and the compressibility of FeH_x under high pressure have been extensively studied. Stoichiometric FeH_x ($x \sim 1.0$) has been confirmed to show three types of high-pressure polymorph: body-centered cubic (*bcc*), double hexagonal close-packed (*dhcp*), and face-centered cubic (*fcc*) phases of FeH_x (e.g., Sakamaki et al., 2009). FeH_2, FeH_3, and FeH_5 were recently discovered at high pressures and high hydrogen concentration conditions (Pépin et al., 2014, 2017). Because of hydrogen's low atomic weight, about 1 wt.% (36 at.%) of hydrogen in Fe would be enough to account for the density deficit in the core (Poirier, 1994; Umemoto and Hirose, 2015). The required hydrogen content in the core becomes smaller in the case of Fe hydride with the other candidate light elements such as Si and S (Shibazaki et al., 2011; Tagawa et al., 2016; Terasaki et al., 2011).

The electrical and thermal conductivity of the Earth's core is crucial for understanding the cooling history and thermal evolution of the Earth's interior (e.g., Labrosse, 2015). Recent studies reported that the conductivity of pure Fe is much higher than we have ever thought (de Koker et al., 2012; Gomi et al., 2013; Ohta et al., 2016; Pozzo et al., 2012), but contrasting results exist (Konôpková et al., 2016; Xu et al., 2018). Light elements and dilute Ni in the core act as additional electron scatterers in the Fe

* Corresponding author.
E-mail address: k-ohta@geo.titech.ac.jp (K. Ohta).

https://doi.org/10.1016/j.crte.2018.05.004
1631-0713/

alloy, and thus reduce the conductivity of the host metal. Impurity effects of Si, O, S, C, and Ni on Fe conductivity have already been investigated at high pressures (de Koker et al., 2012; Gomi and Hirose, 2015; Gomi et al., 2013, 2016; Pozzo et al., 2012; Seagle et al., 2013; Secco, 2017; Suehiro et al., 2017; Wagle et al., 2018; Zhang et al., 2018). However, the effect of hydrogen solution on the conductivity of Fe and Fe–Ni alloy remains unknown.

In this study, we measured high-pressure (P) and temperature (T) electrical resistivity (the reciprocal of electrical conductivity) values of *fcc* FeH_x up to 65 GPa and *fcc* $FeNiH_x$ at 47 GPa in a laser-heated diamond anvil cell (LHDAC). The hydrogen content (x) in our samples was estimated based on synchrotron X-ray diffraction (XRD) studies. From the obtained results, we constrain the transport properties in the Fe–H system at high P–T conditions. Since the impurity resistivity of hydrogen in Fe is found to be very small, hydrogen would not play an important role in the conductivity of the Earth's core.

2. Experimental methods

Fe (–Ni) hydrides with *fcc* structure were prepared by laser heating of Fe or Fe–Ni alloy in the presence of an internal hydrogen source in a LHDAC with 300 μm culet anvils. The host metals were the pure Fe foil (99.99% purity) and the foil of Fe containing 10 wt.% (9.56 at.%) Ni, which are the same products as those used in the literature (Gomi and Hirose, 2015; Gomi et al., 2013; Ohta et al., 2016). Hydrogen was supplied into the sample chamber by a decomposition reaction of paraffin (C_nH_{2n+2}, $n > 5$). This method has been used for the successful synthesis of *fcc* FeH_x in a LHDAC (Narygina et al., 2011; Thompson et al., 2018). The paraffin also served as a pressure transmitting medium and thermal insulator against diamond anvils.

All the experiments were performed at BL10XU, SPring-8. A monochromatic X-ray beam with an energy of 30 keV was directed at the sample. Angle-dispersive XRD spectra were acquired on a flat-panel detector (PerkinElmer). The sample-to-flat-panel distance, the wavelength of the incident X-ray, and the flat panel geometry were calibrated with a CeO_2 standard. The high temperature was generated by using a couple of 100 W Yb-fiber lasers. We collected thermal radiation from the heated sample and analyzed it to convert the temperature (Ohishi et al., 2008). The pressures were determined at 300 K from a spectrum of ruby fluorescence (Dorogokupets and Oganov, 2007) for FeH_x alloys and the diamond Raman edge method (Akahama and Kawamura, 2006) for $FeNiH_x$ alloy.

Methods for the high P–T electrical resistivity measurements in a LHDAC are similar to our previous studies (Ohta et al., 2016; Suehiro et al., 2017). The Fe and Fe–10 wt.% Ni foils were shaped into the sample with four electrodes by using a focused-ion-beam (FIB) apparatus. The shaped metal foil sample and the paraffin were loaded into a sample chamber at the center of an insulated gasket consisting of Re and cBN. Four electrical leads made of Pt were connected to each Fe (or Fe–Ni) electrode outside the sample chamber. The electrical resistance of the sample was measured by the four-terminal method using a SourceMeter (Keithley 2450) under a constant direct current of 100 mA. Since temperature heterogeneity in a laser-heated area of the sample generates thermo-electric power, we measured the voltages of samples by passing direct current from both current directions and averaging these two voltage values to eliminate the effect of thermo-electric power.

We use an empirical method proposed by Fukai (1992) to estimate hydrogen content (x) in the prepared Fe_{H_x} and $FeNi_{H_x}$:

$$x = \frac{V_{M_{H_x}} - V_M}{\Delta V_H}, \quad (1)$$

in which $V_{M_{H_x}}$ and V_M are the lattice volume per number of metal atoms of the metal hydride and the host metal, respectively, and ΔV_H is a predetermined volume expansion due to an interstitial hydrogen. In this study, $V_{fcc\ FeHx}$ and $V_{fcc\ FeNiH_x}$ at each pressure were directly obtained by the XRD experiments. We used the P–V–T equation of state (EoS) of *fcc* Fe reported by Komabayashi (2014) for $V_{fcc\ Fe}$. The atomic volume of *fcc* Fe–10 wt.% Ni ($V_{fcc\ FeNi}$) was estimated using the thermoelastic parameters reported by Funamori et al. (1996) and Basinski et al. (1955). We assume that ΔV_H is the same as $\Delta V_D = 2.21$ Å^3, which was determined from the recent neutron diffraction experiment for *fcc* FeD_x (Machida et al., 2014).

3. Results

We first synthesized the Fe (–Ni) hydrides at around 50–60 GPa and 1700 K for all runs that were monitored by

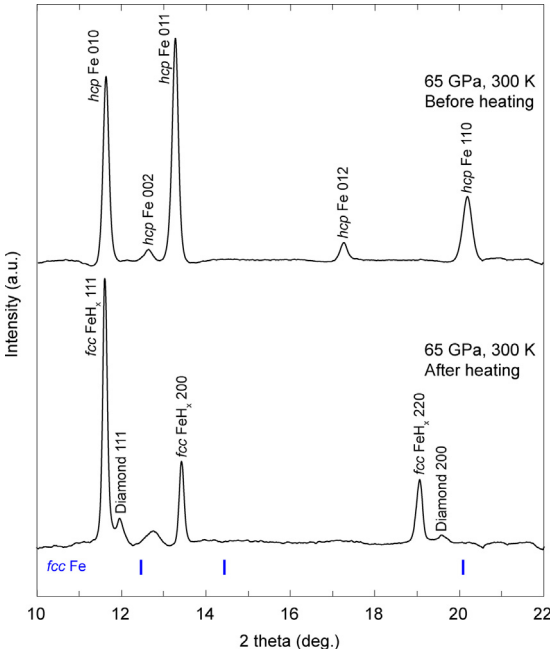

Fig. 1. Representative XRD patterns obtained before and after laser heating for an Fe sample and paraffin pressure medium in the first run. (Upper pattern) The diffraction lines of *hcp* Fe obtained at 65 GPa before laser heating. (Lower) XRD peaks from *fcc* FeH_x and diamond, which are reaction products of Fe and paraffin after laser heating. The calculated XRD peak positions of *fcc* Fe at 65 GPa and 300 K are shown by blue bars.

XRD (Fig. 1). The obtained XRD patterns indicate that the *hcp* Fe sample and paraffin reacted and formed Fe carbides (Fe_3C and Fe_7C_3) soon after the beginning of laser heating, and then the Fe carbides disappeared, and *fcc* FeH_x and the diamond formed in one hour. Our experiments perfectly reproduced the previous study of *fcc* FeH_x formation (Narygina et al., 2011). Incorporation of hydrogen expands the Fe lattice so that the lattice volume of *fcc* FeH_x is much larger than that of *fcc* Fe at equivalent conditions.

After the formation of Fe (–Ni) hydrides at around 50–60 GPa, we changed the pressures to perform electrical resistivity measurements on *fcc* FeH_x at 34, 39, and 65 GPa and on *fcc* $FeNiH_x$ at 47 GPa, respectively. We did not conduct the resistivity measurements at higher pressures to avoid the occurrence of the Fe polyhydrides, although the stable *P*–*T* conditions of the Fe polyhydrides remain unknown (Pépin et al., 2014, 2017). The results of the resistivity measurements are shown in Fig. 2. For comparison, we also plot the resistivity data of Fe at 26 GPa up to 2610 K (Ohta et al., 2016) and the calculated resistivity values of Fe and Fe–10 wt.% Ni alloy based on the model proposed by Gomi and Hirose (2015). This model considers the resistivity saturation phenomenon and Matthiessen's rule for Ni impurity as follows. The resistivity saturation is expressed by the shunt resistor model (Wiesmann et al., 1977):

$$\frac{1}{\rho_{\mathrm{total}}(V,T)} = \frac{1}{\rho_{\mathrm{ideal}}(V,T)} + \frac{1}{\rho_{\mathrm{sat}}(V)}, \tag{2}$$

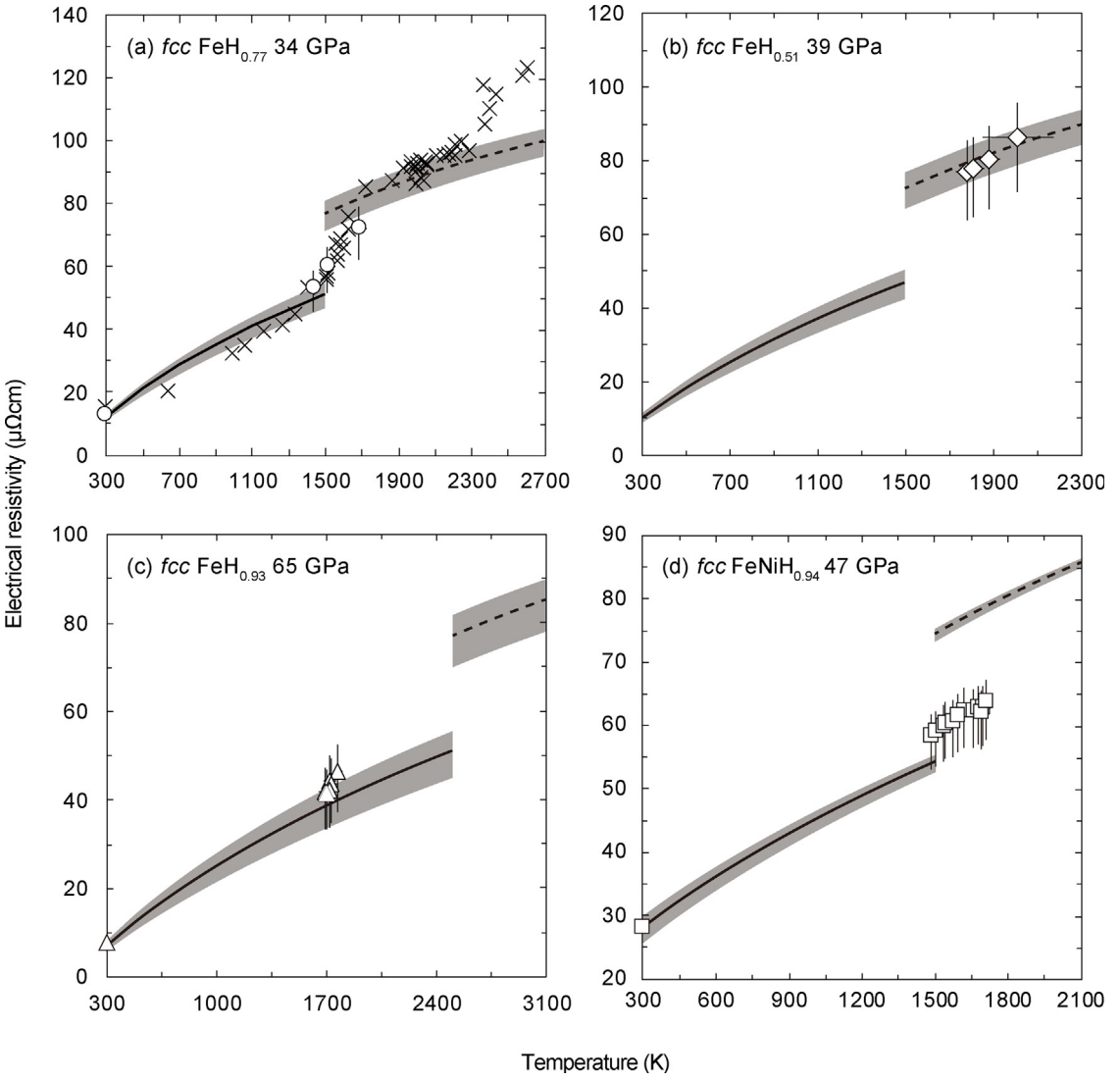

Fig. 2. High-*T* electrical resistivity values of (a) *fcc* $FeH_{0.77}$ at 34 GPa, (b) *fcc* $FeH_{0.51}$ at 39 GPa, (c) *fcc* $FeH_{0.93}$ at 65 GPa, and (d) *fcc* $FeNiH_{0.94}$ at 47 GPa shown as open symbols in each panel. The crosses in Fig. 2a indicate the reported resistivity data of Fe at 26 GPa (Ohta et al., 2016). Black lines with gray band are the calculated resistivity values of *hcp* Fe and *hcp* Fe–10 wt.% Ni alloy using the model proposed in the literature (Eq. (2)–(5)) (Gomi et al., 2013; Gomi and Hirose, 2015). Black broken lines are for *fcc* Fe and *fcc* Fe–10 wt.% Ni alloy. The temperatures of *hcp* to *fcc* phase transition at each pressure are taken from Anzellini et al. (2013) for Fe and from Komabayashi et al. (2012) for the Fe–10 wt.% Ni alloy.

where $\rho_{sat}(V)$ is the volume-dependent saturation resistivity (Gomi et al., 2013),

$$\rho_{sat}(V) = 168\left(\frac{V}{V_0}\right)^{\frac{1}{3}}(\mu\Omega\times\mathrm{cm}) \quad (3)$$

and $\rho_{ideal}(V,T)$ is the ideal resistivity described by the Matthiessen rule and the Bloch–Grüneisen law:

$$\rho_{ideal}(V,T) = \rho_{Fe}(V,T) + \sum_i x_i\rho_i(V) \quad (4)$$

where $\rho_i(V)$ and χ_i are impurity resistivity and its concentration, and $\rho_{Fe}(V,T)$ is the F resistivity computed from the Bloch–Grüneisen law:

$$\rho_{Fe}(V,T) = B(V)\left(\frac{T}{\Theta_D(V)}\right)^5\int_0^{\frac{\Theta_D(V)}{T}}\frac{z^5dz}{(\exp(z)-1)(1-\exp(-z))}, \quad (5)$$

where $\Theta_D(V)$ is the Debye temperature and $B(V)$ is a material constant. The impurity resistivity of Ni has been determined using the following equation (Gomi and Hirose, 2015):

$$\rho_{Ni(V)} = 7250\left(3.51-\frac{V}{V_0}\right)^{-8.06}(\Omega\times\mathrm{cm/at.\%}). \quad (6)$$

The EoS of *hcp* Fe (Dewaele et al., 2006) is used to calculate the values of V and $\Theta_D(V)$. We assume a twofold increase of the $\rho_{Fe}(V,T)$ due to the *hcp–fcc* transition as in 26 GPa data (Fig. 2a).

In the first run at 65 GPa, the resistance of the synthesized *fcc* FeH_x sample increased by 2% compared to that of *hcp* Fe, which was measured before heating at 300 K. The hydrogen content of this sample was calculated as $x = 0.93$ using Eq. (1). Considering the increase in the resistance and the volume expansion due to the *fcc* $FeH_{0.93}$ formation, we converted the high-*P*/room-*T* electrical resistivity of *hcp* Fe determined by Gomi et al. (2013) to high-*P*/room-*T* resistivity of the *fcc* $FeH_{0.93}$ at 65 GPa. High-*P*/high-*T* resistivity of the *fcc* $FeH_{0.93}$ was calculated from the ratio of resistance measured at high temperature up to 1770 K to that measured at room temperature, multiplied by the high-*P*/room-*T* resistivity of the *fcc* $FeH_{0.93}$ (Fig. 2c). As shown in Fig. 2c, the resistivity of *fcc* $FeH_{0.93}$ is 5–18% higher than that of *hcp* Fe, but they are comparable within the experimental uncertainty.

According to the previous studies, the hydrogen solubility in *fcc* Fe and the *fcc* Fe–Ni alloy decreases with increasing the temperature in a certain pressure range (Hiroi et al., 2005; Shibazaki et al., 2014). Therefore, we expected to be able to vary the hydrogen content in the pre-synthesized $FeH_{0.93}$ to make the pressure and temperature conditions deviate from those in the pre-synthesis situation. Thus, we decompressed

Table 1
Experimental conditions, observed volumes, hydrogen contents, and electrical resistivities.

Run	*P* (GPa)[a]	*T* (K)	Phase	Observed lattice *V* (Å^3)	*x*	Resistivity (μΩ·cm)
1	65	300	*fcc* FeH_x	44.51 (6)	0.93	8.0 (+1.0/−1.6)
		1690 (40)	*fcc* FeH_x			41.8 (+5.4/−8.4)
		1700 (30)	*fcc* FeH_x			41.6 (+5.4/−8.3)
		1720 (30)	*fcc* FeH_x			42.2 (+5.5/−8.4)
		1720 (40)	*fcc* FeH_x			44.4 (+5.8/−8.9)
		1730 (40)	*fcc* FeH_x			43.7 (+5.7/−8.7)
		1770 (30)	*fcc* FeH_x			46.5 (+6.0/−9.3)
	After decompression and annealing					
	34	300	*fcc* FeH_x	46.13 (4)	0.77	12.6 (+1.3/−1.8)
		1440 (30)	*fcc* FeH_x			53.3 (+5.3/−7.5)
		1520 (30)	*fcc* FeH_x			60.1 (+6.0/−8.4)
		1690 (30)	*fcc* FeH_x			72.0 (+7.2/−10.1)
2	48	300	*fcc* FeH_x	44.95 (14)	0.81	9.5 (+1.1/−1.4)
	After decompression and annealing					
	39	300	*fcc* FeH_x	43.27 (8)	0.51	n.d.
		1780 (50)	*fcc* FeH_x			76.9 (+8.5/−13.1)
		1810 (50)	*fcc* FeH_x			77.9 (+8.6/−13.3)
		1880 (50)	*fcc* FeH_x			80.5 (+8.9/−13.7)
		2010 (160)	*fcc* FeH_x			86.2 (+9.5/−14.7)
3	47	300	*fcc* $FeNiH_x$	46.21 (6)	0.94	28.1 (+1.6/−2.6)
		1490 (20)	*fcc* $FeNiH_x$			58.3 (+3.3/−5.4)
		1500 (20)	*fcc* $FeNiH_x$			59.0 (+3.3/−5.4)
		1530 (20)	*fcc* $FeNiH_x$			59.9 (+3.4/−5.5)
		1540 (20)	*fcc* $FeNiH_x$			60.3 (+3.4/−5.5)
		1570 (20)	*fcc* $FeNiH_x$			60.6 (+3.4/−5.6)
		1590 (20)	*fcc* $FeNiH_x$			61.5 (+3.5/−5.6)
		1620 (20)	*fcc* $FeNiH_x$			62.4 (+3.5/−5.7)
		1660 (30)	*fcc* $FeNiH_x$			62.3 (+3.5/−5.7)
		1680 (30)	*fcc* $FeNiH_x$			62.8 (+3.5/−5.8)
		1690 (30)	*fcc* $FeNiH_x$			62.0 (+3.5/−5.7)
		1700 (30)	*fcc* $FeNiH_x$			62.3 (+3.5/−5.8)
		1710 (20)	*fcc* $FeNiH_x$			63.7 (+3.6/−5.9)

n.d.: not determined.
[a] Pressures were determined from the ruby method in Runs 1 and 2 and from the diamond Raman method in Run 3.

the same sample to 34 GPa, and annealed it at about 1700 K. After annealing, the hydrogen content decreased to $x = 0.77$ as we had expected, implying that the process of hydrogen dissolution into *fcc* Fe is exothermic (x decreases with increasing T) at 34 GPa. We determined the resistivity values of *fcc* $FeH_{0.77}$ at 34 GPa up to 1690 K (Fig. 2a). These values are intermediate between those of *hcp* and *fcc* Fe in the same P–T conditions.

The resistivity of the *fcc* FeH_x was also examined at 39 GPa up to 2100 K in a different run (Fig. 2b). We synthesized the *fcc* FeH_x at 48 GPa and 1750 K in 1 hour, and then decreased the pressure to 39 GPa and annealed it. We found that this sample's x value was 0.51 after annealing. The obtained resistivity of *fcc* $FeH_{0.51}$ is very similar to that of *fcc* Fe, conversely to *hcp* Fe, which is different from the case for *fcc* FeH_x, with a higher hydrogen concentration, as shown in the first run (Fig. 2a, c).

A similar experiment was also carried out on an Fe–Ni-H system (Fig. 2d). *fcc* Fe–Ni hydride was formed at 47 GPa and around 1700 K in 1.5 h. Its hydrogen content was determined as $FeNiH_{0.94}$. The reported experimental result (Gomi and Hirose, 2015) was taken as the reference value of the resistivity of Fe–10 wt.% Ni alloy at 47 GPa and 300 K. This nearly stoichiometric *fcc* Fe–Ni hydride showed a resistivity value similar to that of *hcp* Fe with 10 wt.% Ni alloy, which was calculated using the model proposed by Gomi and Hirose (2015) (Table 1).

4. Discussion

dhcp FeH_x ($x \sim 1.0$) has been confirmed to have its metallic property denoted by the resistivity increase with increasing temperature (Matsuoka et al., 2011), but it is unknown whether other phases of the Fe hydride are metallic or insulator. The present study revealed the electrical transport properties of nearly stoichiometric *fcc* FeH_x and $FeNiH_x$ ($x \sim 1.0$), and nonstoichiometric *fcc* FeH_x ($x = 0.77$ and 0.51) at high pressures and high temperatures, and all the examined *fcc* Fe (–Ni) hydrides showed a metallic nature (Fig. 2). In addition, our results indicate that hydrogen-rich *fcc* FeH_x ($x > 0.5$) becomes more conductive with increasing the hydrogen content.

The core density deficit requires about 1 wt.% (36 at.%) of hydrogen as the sole light element in the core (Poirier, 1994; Umemoto and Hirose, 2015). Therefore, in order to discuss the effect of hydrogen on the Earth's core conductivity, the impurity resistivity of the minor amount of hydrogen in Fe is important to constrain. Note, however, that the Matthiessen's rule is only valid at a low impurity concentration up to about 20 at.% in general (Gomi et al., 2016). In some metallic binary continuous solid solutions, the dependence of the resistivity on the composition is characterized by a convex parabolic curve. We predicted the resistivity in an Fe–FeH system from the present data and the form of Nordheim's rule:

$$\rho_{FeH_x} = (1-x)\rho_{Fe} + x\rho_{FeH_{1.0}} + kx(1-x), \quad (7)$$

where ρ_{Fe} and $\rho_{FeH_{1.0}}$ are the electrical resistivities of Fe and $FeH_{1.0}$, respectively, and k is a positive constant that depends on the alloy system. Here we assume the resistivity of *fcc* $FeH_{1.0}$ is the same as that of *hcp* Fe based on our results (Fig. 2). Fig. 3 shows the predicted relation of the resistivity in a *fcc* Fe–*fcc* $FeH_{1.0}$ system at 34 GPa and 1690 K with that at 39 GPa and 2100 K. The k values in Eq. (7), i.e. 61 at 34 GPa and 55 at 39 GPa, fit our experimental data. The volume-dependent impurity resistivity values of Si, Ni, S, and C (ρ_{Si}, ρ_{Ni}, ρ_S, and ρ_C) have been experimentally determined (Gomi and Hirose, 2015; Gomi et al., 2016; Suehiro et al., 2017; Zhang et al., 2018). The obtained ρ_{Si}, ρ_{Ni}, ρ_S, and ρ_C are 7.2, 2.9, 4.6, and 12.1 μΩ·cm/at% at 34 GPa, and are 6.8, 2.8, 4.4, and 11.4 μΩ·cm/at% at 39 GPa, respectively. We calculated the resistivity values of *fcc* Fe with Si, Ni, S, and C using their impurity resistivity values and Eqs. (2)–(5) (Fig. 3). The effect of a small amount of hydrogen on Fe resistivity is likely to be weaker than that of these four elements. Gomi et al. (2013) also predicted the impurity resistivity of O in Fe (ρ_O) based on the Norbury–Linde rule. According to this rule, the ρ_O is one-fourth of the ρ_{Si}, although the validity of the Norbury–Linde rule for iron alloys at high pressures is unclear. To the best of our knowledge, the strongest

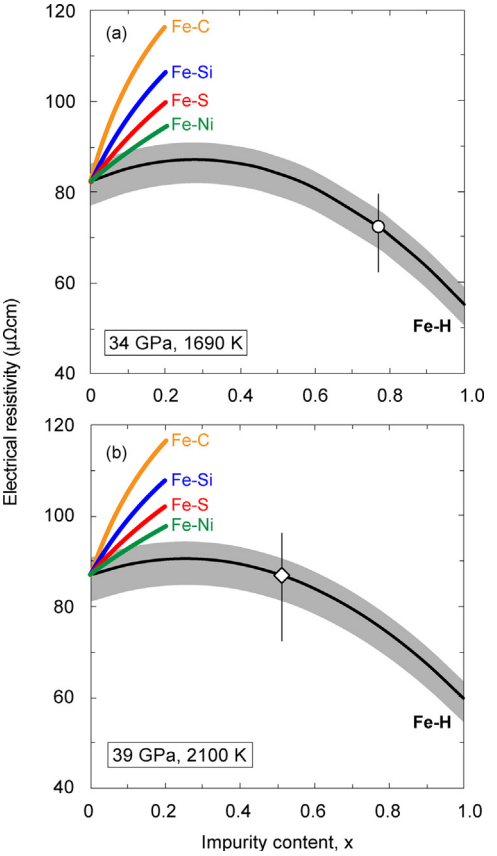

Fig. 3. The electrical resistivity in an FeH_x system (a) at 34 GPa and 1690 K, and (b) at 39 GPa and 2100 K. The open symbols are the present data (Fig. 2a, b). The black lines with gray band indicate the resistivity of FeH_x as a function of the hydrogen content x estimated from the form of Nordheim's rule. The effects of C, Si, S, and Ni on the Fe resistivity are calculated from Matthiessen's rule and the saturation model (Eq. (2)–(5)). Orange, Fe–C alloy from Zhang et al. (2018); blue, Fe–Si alloy from Gomi et al. (2016); red, Fe–S alloy from Suehiro et al. (2017); green, Fe–Ni alloy from Gomi and Hirose (2015).

impurity scatterer in iron among the core light element candidates would be carbon, while the weakest one would be hydrogen in the present experimental pressures range.

Incorporation of hydrogen significantly decreases the density and the melting temperature of Fe, even when in low quantities. Such characteristics of hydrogen appear to elucidate the density deficit of the core (e.g., Badding et al., 1991) and the low solidus temperature of the pyrolytic lowermost mantle (Nomura et al., 2014). However, the present study indicates the minor contribution of hydrogen incorporation in the core to electrical conductivity, and hence the electronic thermal conductivity. The 1 wt.% (36 at.%) hydrogen incorporation enhances the electrical resistivity of Fe a few % at 39 GPa and 2100 K (Fig. 3b). Hydrogen impurity resistivity would decrease with increasing pressure, as it does for other light elements (Gomi et al., 2016; Suehiro et al., 2017; Zhang et al., 2018), so that the influence of hydrogen in the Earth's core resistivity should be smaller. The hydrogen content in the uppermost core could increase as a result of the interaction between the core and hydrous minerals such as the δ-AlOOH, phase H of $MgSiO_4H_2$ and pyrite-type FeOOH in the mantle and subducting slab (Nishi et al., 2014, 2017; Terasaki et al., 2012), which would induce the compositional layering in the outer core (Helffrich, 2014). However, the increase in hydrogen solubility at the top of the core has a very limited influence on the core conductivity and thus the thermal evolution of the core.

Acknowledgments

We thank Dr. Takahiro Matsuoka for discussion. *In situ* high *P*–*T* synchrotron XRD measurements were performed at BL10XU, SPring-8 (proposals No. 2014B0087, 2015A0087, and 2017B0072). This work was supported by JSPS KAKENHI, Grant Numbers 15H05827 and 17H04861.

References

Akahama, Y., Kawamura, H., 2006. Pressure calibration of diamond anvil Raman gauge to 310 GPa. J. Appl. Phys. 100, 043516.
Anzellini, S., Dewaele, A., Mezouar, M., Loubeyre, P., Morard, G., 2013. Melting of iron at Earth's inner core boundary based on fast X-ray diffraction. Science 340, 464–466.
Badding, J.V., Hemley, R.J., Mao, H.-K., 1991. High-pressure chemistry of hydrogen in metals: in situ study of iron hydride. Science 253, 421–424.
Basinski, Z.S., Hume-Rothery, W., Sutton, A.L., 1955. The lattice expansion of iron. Proc. R. Soc. A 229, 459–467.
Birch, F., 1952. Elasticity and constitution of the Earth's interior. J. Geophys. Res. 52, 227–286.
de Koker, N., Steinle-Neumann, G., Vlcek, V., 2012. Electrical resistivity and thermal conductivity of liquid Fe alloys at high P and T, and heat flux in Earth's core. Proc. Natl. Acad. Sci. USA 109, 4070–4073.
Dewaele, A., Loubeyre, P., Occelli, F., Mezouar, M., Dorogokupets, P., Torrent, M., 2006. Quasihydrostatic equation of state of iron above 2 Mbar. Phys. Rev. Lett. 97, 215504.
Dorogokupets, P.I., Oganov, A.R., 2007. Ruby, metals, and MgO as alternative pressure scales: a semiempirical description of shock-wave, ultrasonic, X-ray, and thermochemical data at high temperatures and pressures. Phys. Rev. B 75, 024115.
Fukai, Y., 1992. Some properties of the Fe–H system at high pressures and temperatures, and their implications for the Earth's core. In: Syono, Y., Manghnani, M.H. (Eds.), High-Pressure Research: Application to Earth and Planetary Sciences. TERRAPUB, Washington, DC, pp. 373–385.
Fukai, Y., Akimoto, S., 1983. Hydrogen in the earth's core. Experimental approach. Proc. Japan Acad. Ser. B 59, 158–162.
Funamori, N., Yagi, T., Uchida, T., 1996. High-pressure and high-temperature in situ X-ray diffraction study of iron to above 30 GPa using MA8-type apparatus. Geophys. Res. Lett. 23, 953–956.
Gomi, H., Ohta, K., Hirose, K., Labrosse, S., Caracas, R., Verstraete, M.J., Hernlund, J.W., 2013. The high conductivity of iron and thermal evolution of the Earth's core. Phys. Earth Planet. Inter. 224, 88–103.
Gomi, H., Hirose, K., 2015. Electrical resistivity and thermal conductivity of hcp Fe–Ni alloys under high pressure: Implications for thermal convection in the Earth's core. Phys. Earth Planet. Inter. 247, 2–10.
Gomi, H., Hirose, K., Akai, H., Fei, Y., 2016. Electrical resistivity of substitutionally disordered hcp Fe–Si and Fe–Ni alloys: chemically-induced resistivity saturation in the Earth's core. Earth Planet. Sci. Lett. 451, 51–61.
Helffrich, G., 2014. Outer core compositional layering and constraints on core liquid transport properties. Earth Planet. Sci. Lett. 391, 256–262.
Hiroi, T., Fukai, Y., Mori, K., 2005. The phase diagram and superabundant vacancy formation in Fe–H alloys revisited. J. Alloy Compd. 404, 252–255.
Iizuka-Oku, R., Yagi, T., Gotou, H., Okuchi, T., Hattori, T., Sano-Furukawa, A., 2017. Hydrogenation of iron in the early stage of Earth's evolution. Nat. Commun. 8, 14096.
Komabayashi, T., 2014. Thermodynamics of melting relations in the system Fe–FeO at high pressure: implications for oxygen in the Earth's core. J. Geophys. Res. 119, 4164–4177.
Komabayashi, T., Hirose, K., Ohishi, Y., 2012. In situ X-ray diffraction measurements of the *fcc–hcp* phase transition boundary of an Fe–Ni alloy in an internally heated diamond anvil cell. Phys. Chem. Miner. 39, 329–338.
Konôpková, Z., McWilliams, R., Gómez-Pérez, N., Goncharov, A., 2016. Direct measurement of thermal conductivity in solid iron at planetary core conditions. Nature 534, 99–101.
Labrosse, S., 2015. Thermal evolution of the core with a high thermal conductivity. Phys. Earth Planet. Inter. 247, 36–55.
Machida, A., Saitoh, H., Sugimoto, H., Hattori, T., Sano-Furukawa, A., Endo, N., Katayama, Y., Iizuka, R., Sato, T., Matsuo, M., Orimo, S., Aoki, K., 2014. Site occupancy of interstitial deuterium atoms in face-centred cubic iron. Nat. Commun. 5, 5063.
Mao, W., Sturhahn, W., Heinz, D., Mao, H., Shu, J., Hemley, R., 2004. Nuclear resonant X-ray scattering of iron hydride at high pressure. Geophys. Res. Lett. 31, L15618.
Matsuoka, T., Hirao, N., Ohishi, Y., Shimizu, K., Machida, A., Aoki, K., 2011. Structural and electrical transport properties of FeH_x under high pressures and low temperatures. High Pressure Res. 31, 64–67.
Narygina, O., Dubrovinsky, L., McCammon, C., Kurnosov, A., Kantor, I., Prakapenka, V., Dubrovinskaia, N., 2011. X-ray diffraction and Mössbauer spectroscopy study of fcc iron hydride FeH at high pressures and implications for the composition of the Earth's core. Earth Planet. Sci. Lett. 307, 409–414.
Nishi, M., Irifune, T., Tsuchiya, J., Tange, Y., Nishihara, Y., Fujino, K., Higo, Y., 2014. Stability of hydrous silicate at high pressures and water transport to the deep lower mantle. Nature Geosci. 7, 224–227.
Nishi, M., Kuwayama, Y., Tsuchiya, J., Tsuchiya, T., 2017. The pyrite-type high-pressure form of FeOOH. Nature 547, 205–208.
Nomura, R., Hirose, K., Uesugi, K., Ohishi, Y., Tsuchiyama, A., Miyake, A., Ueno, Y., 2014. Low core-mantle boundary temperature inferred from the solidus of pyrolite. Science 343, 522–525.
Ohishi, Y., Hirao, N., Sata, N., Hirose, K., Takata, M., 2008. Highly intense monochromatic X-ray diffraction facility for high-pressure research at SPring-8. High Pressure Res. 28, 163–173.
Ohta, K., Kuwayama, Y., Hirose, K., Shimizu, K., Ohishi, Y., 2016. Experimental determination of the electrical resistivity of iron at Earth's core conditions. Nature 534, 95–98.
Pépin, C., Dewaele, A., Geneste, G., Loubeyre, P., Mezouar, M., 2014. New iron hydrides under high pressure. Phys. Rev. Lett. 113, 265504.
Pépin, C.M., Geneste, G., Dewaele, A., Mezouar, M., 2017. Synthesis of FeH5: a layered structure with atomic hydrogen slabs. Science 357, 382–385.
Poirier, J.-P., 1994. Light elements in the Earth's outer core: a critical review. Phys. Earth Planet. Inter. 85, 319–337.
Pozzo, M., Davies, C., Gubbins, D., Alfè, D., 2012. Thermal and electrical conductivity of iron at Earth's core conditions. Nature 485, 355–358.
Sakamaki, K., Takahashi, E., Nakajima, Y., Nishihara, Y., Funakoshi, K., Suzuki, T., Fukai, Y., 2009. Melting phase relation of FeHx up to 20 GPa: Implication for the temperature of the Earth's core. Phys. Earth Planet. Inter. 174, 192–201.
Seagle, C., Cottrell, E., Fei, Y., Hummer, D., Prakapenka, V., 2013. Electrical and thermal transport properties of iron and iron-silicon alloy at high pressure. Geophys. Res. Lett. 40, 5377–5381.

Secco, R., 2017. Thermal conductivity and Seebeck coefficient of Fe and Fe–Si alloys: implications for variable Lorenz number. Phys. Earth Planet. Inter. 265, 23–34.

Shibazaki, Y., Ohtani, E., Terasaki, H., Tateyama, R., Sakamaki, T., Tsuchiya, T., Funakoshi, K., 2011. Effect of hydrogen on the melting temperature of FeS at high pressure: implications for the core of Ganymede. Earth Planet. Sci. Lett. 301, 153–158.

Shibazaki, Y., Ohtani, E., Fukui, H., Sakai, T., Kamada, S., Ishikawa, D., Tsutsui, S., Baron, A., Nishitani, N., Hirao, N., Takemura, K., 2012. Sound velocity measurements in dhcp-FeH up to 70 GPa with inelastic X-ray scattering: Implications for the composition of the Earth's core. Earth Planet. Sci. Lett. 313–314, 79–85.

Shibazaki, Y., Terasaki, H., Ohtani, E., Tateyama, R., Nishida, K., Funakoshi, K., Higo, Y., 2014. High-pressure and high-temperature phase diagram for $Fe_{0.9}Ni_{0.1}$–H alloy. Phys. Earth Planet. Inter. 228, 192–201.

Stevenson, D.J., 1977. Hydrogen in the Earth's core. Nature 268, 130–131.

Suehiro, S., Ohta, K., Hirose, K., Morard, G., Ohishi, Y., 2017. The influence of sulfur on the electrical resistivity of hcp iron: Implications for the core conductivity of Mars and Earth. Geophys. Res. Lett. 44, 8254–8259.

Tagawa, S., Ohta, K., Hirose, K., Kato, C., Ohishi, Y., 2016. Compression of Fe–Si–H alloys to core pressures. Geophys. Res. Lett. 43, 3686–3692.

Terasaki, H., Shibazaki, Y., Sakamaki, T., Tateyama, R., Ohtani, E., Funakoshi, K., Higo, Y., 2011. Hydrogenation of FeSi under high pressure. Am. Mineral. 96, 93–99.

Terasaki, H., Ohtani, E., Sakai, T., Kamada, S., Asanuma, H., Shibazaki, Y., Hirao, N., Sata, N., Ohishi, Y., Sakamaki, T., Suzuki, A., Funakoshi, K., 2012. Stability of Fe–Ni hydride after the reaction between Fe–Ni alloy and hydrous phase (δ-AlOOH) up to 1.2 Mbar: possibility of H contribution to the core density deficit. Phys. Earth Planet. Inter. 194–195, 18–24.

Thompson, E., Davis, A., Bi, W., Zhao, J., Alp, E., Zhang, D., Greenberg, E., Prakapenka, V., Campbell, A., 2018. High-pressure geophysical properties of *fcc* phase FeH_x. Geochem. Geophys. Geosys. 19, 305–314.

Umemoto, K., Hirose, K., 2015. Liquid iron-hydrogen alloys at outer core conditions by first-principles calculations. Geophys. Res. Lett. 42, 7513–7520.

Wagle, F., Steinle-Neumann, G., Koker, N., 2018. Saturation and negative temperature coefficient of electrical resistivity in liquid iron-sulfur alloys at high densities from first-principles calculations. Phys. Rev. B 97, 094307.

Wiesmann, H., Gurvitch, M., Lutz, H., Ghosh, A., Schwarz, B., Strongin, M., Allen, P., Halley, J., 1977. Simple model for characterizing the electrical resistivity in A-15 superconductors. Phys. Rev. Lett. 38, 782–785.

Xu, J., Zhang, P., Haule, K., Minar, J., Wimmer, S., Ebert, H., Cohen, R.E., 2018. Thermal conductivity and electrical resistivity of solid iron at Earth's core conditions from first-principles. (ar Xiv:1710.03564).

Zhang, C., Lin, J.-F., Liu, Y., Feng, S., Jin, C., Hou, M., Yoshino, T., 2018. Electrical resistivity of Fe–C alloy at high pressure: effects of carbon as a light element on the thermal conductivity of the Earth's core. J. Geophys. Res. 123, 3564–3577, http://dx.doi.org/10.1029/2017JB015260.